Journal of Rock Mechanics and Geotechnical Engineering 9 (2017) 761–766

Contents lists available at ScienceDirect

Journal of Rock Mechanics and Geotechnical Engineering

journal homepage: www.rockgeotech.org

Full Length Article

Depth factors for undrained bearing capacity of circular footing by numerical approach

Sadok Benmebarek*, Insaf Saifi, Naima Benmebarek

NMISSI Laboratory, Biskra University, BP 145, Biskra, 07000, Algeria

ARTICLE INFO

Article history:
Received 26 August 2016
Received in revised form
3 December 2016
Accepted 2 January 2017
Available online 24 May 2017

Keywords:
Circular footing
Bearing capacity
Embedment depth
Numerical modeling
Plasticity

ABSTRACT

The undrained vertical bearing capacity of embedded foundation has been extensively studied using analytical and numerical methods. Through comparing the results of a circular embedded foundation in the literature, a significant difference between the bearing capacity factors and depth factors is observed. Based on the previous research findings, numerical computations using FLAC code are carried out in this study to evaluate the undrained bearing capacity of circular foundations with embedment ratios up to five for different base and side foundation roughness conditions. Unlike the foundation base, the roughness of the foundation side has a significant effect on the bearing capacity. The comparison of the present results with numerical studies available in the literature shows that the discrepancy is related to the procedures used to simulate the foundation side interface conditions and to the estimation of the bearing capacity.

1. Introduction

The bearing capacity for both strip and circular footings on undrained clay has already been one of the hot topics in geotechnical engineering for researchers and practical engineers. In offshore regions, foundations in soft marine deposits as deeply penetrated spudcan, skirted and caisson foundations are often considered as circular embedded foundations. In most cases, it is important to take into account the embedment depth which often exceeds the footing diameter.

Undrained vertical bearing capacity of embedded foundations has been first extensively studied through experimental and analytical methods for a wide range of foundation–soil interface conditions (Terzaghi, 1943; Meyerhof, 1951; Skempton, 1951; Hansen, 1970; Tani and Craig, 1995; Martin, 2001; Martin and Randolph, 2001; Houlsby and Martin, 2003), while numerical investigations of the bearing capacity of embedded footings have been reported by Hu et al. (1999), Salgado et al. (2004), Edwards et al. (2005), Gourvenec and Mana (2011), and Nguyen and Merifield (2012). By using the finite element method, Hu et al. (1999) investigated the undrained bearing capacities of skirted circular rigid foundations with embedment depth up to five times the foundation diameter (D) for a displacement of 0.3D in a nonhomogeneous soil. The results showed a difference in bearing capacity between rough and smooth side cases, which increases with the increasing depth ratio. Salgado et al. (2004) studied the two- and three-dimensional bearing capacities of embedded strip, square, circular and rectangular foundations in clay with embedment ratios up to five using the finite element limit analysis approach. The footing base was assumed rough. The collapse load was expressed in terms of the vertical load transmitted to the soil at the base of the footing. Edwards et al. (2005) reported the finite element analyses of rough circular foundation with embedment ratios up to four for a displacement of 0.3D in undrained homogeneous soil. The footing base was assumed rough but the vertical side of the footing was represented to be both rough and smooth. A uniform vertical displacement was applied to the nodes along the base and side boundaries until failure. The ultimate load on the footing was then calculated as the sum of the vertical reaction forces along the footing base. Gourvenec and Mana (2011) used finite element and limit analysis to estimate bearing capacity factors for rigid strip and circular foundations with embedment ratios up to unity over a range of foundation–soil interface roughness and a practical range of linear soil strength profiles from uniform with depth to essentially normally consolidated. The foundations were modeled as a rigid block with a single load reference point located along the midline of the foundation at foundation level. Foundation

* Corresponding author.
E-mail address: sadok_benmebarek@yahoo.com (S. Benmebarek).
Peer review under responsibility of Institute of Rock and Soil Mechanics, Chinese Academy of Sciences.

http://dx.doi.org/10.1016/j.jrmge.2017.01.003

load was applied by a vertical velocity prescribed at the load reference point. Unfortunately, the vertical load transmitted to the load reference point was used to compute the equivalent bearing capacity. More recently, finite element analysis was used by Nguyen and Merifield (2012) to predict the undrained bearing capacities of strip, square and circular footings embedded in clay. The interactions between the soil and the base of the footings as well as the sides were modeled as rough where interface of footing sides and soil has just vertical displacement only. To determine the collapse load of the footing, a uniform vertical prescribed displacement was applied to all those nodes on the footing. The nodal contact forces along the footing were summed to compute the equivalent bearing capacity.

When the results of a circular footing in the literature are compared, a significant difference between the bearing capacity factors and depth factors is observed. From this review, this could be attributed mainly to the procedures used to simulate the loading and the effect of the foundation side interface conditions in various studies. It can be noted that for Salgado et al. (2004), Edwards et al. (2005), and Nguyen and Merifield (2012), the bearing capacities reported represent only the contribution of the foundation base. However, for Hu et al. (1999) and Gourvenec and Mana (2011), the bearing capacities represent the contribution of both the base and side of the foundation.

To highlight the origin of the divergences in the bearing capacity factor, two analyses were performed using the FLAC code. The first represents the case of contribution of both the base and side of the foundation, whereas the second represents only the contribution of the base.

2. Numerical modeling

This paper deals with the numerical study of bearing capacity of smooth and rough rigid circular embedded footing. The footing is subjected to an axial static load. The geometry and boundary conditions are shown in Fig. 1. Foundation embedment depth to foundation diameter ratio (D_f/D) varies from zero (footing at the ground surface) to five. The axis-symmetric geometry in FLAC is used. The vertical and bottom boundaries are located at a distance of D_f+8r and 16r, respectively, in order to minimize boundary effects, where r is the radius of the footing. The bottom boundary is assumed to be fixed, and the vertical boundaries are constrained in motion in the horizontal direction. Both soil and rigid footing are discretized. Interface elements defined by Coulomb shear strength criterion and encoded in FLAC are placed between soil and footing along the boundary *BCD* (Fig. 1) to simulate different interface conditions. Both combination cases of rough and smooth interfaces base *CD* and vertical side of the footing *BC* are considered.

The model domain for this study is shown in Fig. 2. In the vicinity of the footing, the grid is refined to capture the large gradients in strain. The highest strain gradient will be in the region adjacent to the footing corner. The grid is therefore very fine in this area.

The soil mass assumed to be weightless is modeled using the Mohr–Coulomb constitutive model, in order to be consistent with existing design expressions and the comparative studies described above. Constant undrained strength, $C_u = 100$ kPa, undrained angle of internal friction, $\varphi_u = 0°$, and undrained elastic properties including Young's modulus, E_u, of 50 MPa and Poisson's ratio, ν_u, of 0.495 are assigned to the soil. Interfaces are defined with null friction, cohesion, and normal and shear stiffnesses of 1×10^9 kN/m^3. To model the rough foundation–soil interface, the same soil undrained strength is assigned to interface elements. In the case of a smooth interface, null cohesion is assigned to the interface elements, such that there is essentially no shear stress mobilized along the side of the footing.

The loading of footings is simulated by imposing equal vertical velocities to the nodes of the footing surface represented by the boundary *AB* (Fig. 1) until failure. After running a number of verifications, the magnitude of vertical velocities is finally chosen to be 1×10^{-7} m/s downward, which is small enough to minimize the influence of initial velocity on the results (Itasca, 2007).

Using a FISH function, the ultimate bearing capacity q_u is calculated by dividing the computed ultimate total vertical load by the area of the footing. To explain the divergence in the literature, two manners are investigated for computing the ultimate total vertical load. In the first, the load is calculated as the sum of the vertical reaction forces along the footing level *AB* as expressed by Eq. (1). This load includes the resistance from both the base and the vertical side of the foundation. However, in the second, the load is computed by integrating vertical stresses along the footing base *CD* as indicated by Eq. (2). It does not include the resistance from any shear stresses mobilized along the side of the footing *BC*.

$$q_u(1) = \frac{2\sum(f_i r_i)}{r^2} \tag{1}$$

$$q_u(2) = \frac{2\sum(S_i x_i r_i')}{r^2} \tag{2}$$

where $q_u(1)$ and $q_u(2)$ are the ultimate bearing capacities at the footing top *AB* and base *CD*, respectively; f_i is the reaction force in the vertical direction at footing grid point i; r_i is the associated radius at grid point i; r_i' is the associated radius at center zone i; S_i is

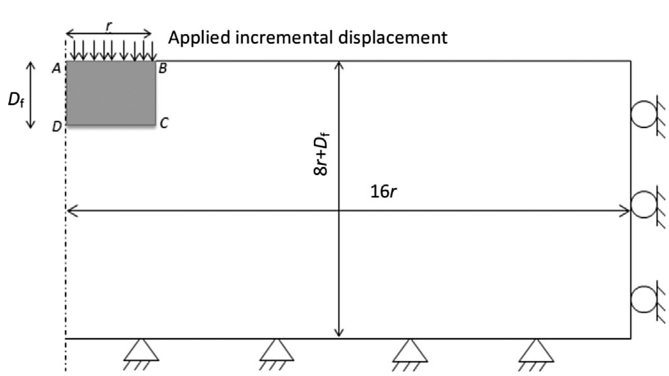

Fig. 1. Model boundary conditions.

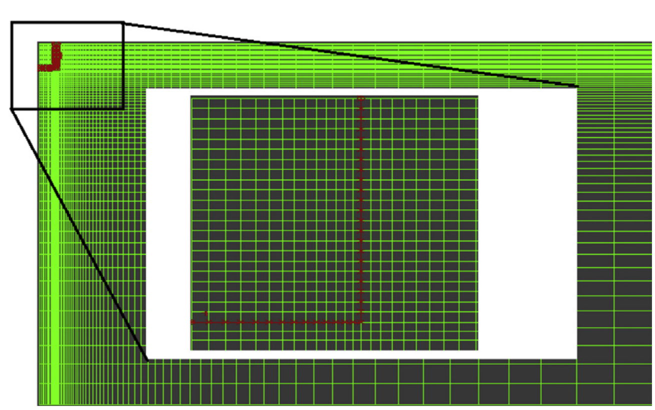

Fig. 2. Typical mesh used in FLAC simulations for $D_f/D = 1$.